https://chemclassjournal.com/
ChemClass Journal Vol. 9 Issue 2 (2025); 547-562
e-ISSN:3092-8214 p-ISSN:3092-8206
DOI: https://doi.org/10.33003/chemclas-2025-0902/178

UV-Vis, XRD, FTIR, SEM, and PSA-Based Characterization of Copper and Iron Nanoparticles Synthesized Using *Spondias mombin* (Hog Plum) Leaf Extract

[1]Eze, Uchenna Samson; [2]*James, Abosede Olubunmi

[1]Department of Chemistry Education, Federal College of Education (Technical) Omoku. Rivers State, Nigeria

** [2]Department of Pure and Industrial Chemistry, University of Port Harcourt, Rivers State, Nigeria*

(*)Corresponding Author's: ezesamson@fcetomoku.edu.ng *Tel: +2348135791204; +2347067986462; +2349154595519
Co-Author's Email: abosede.james@uniport.edu.ng

Abstract

This study examines the biosynthesis and characterization of copper and iron nanoparticles (CuNPs and FeNPs) using *Spondias mombin* leaf extract. The extracts serves as a reducing and stabilizing agent in the formation of nanoparticles. The leaves were collected, identified, and subjected to ethanolic extraction. This was followed by the biosynthesis of nanoparticles via reaction with $Cu(NO_3)_2$ and $FeCl_2$ solutions. However, the reactions was done under controlled heating and stirring resulting to a color change. Color changes from blue to reddish brown indicate CuNPs formation and from clear to dark brown for FeNPs. To characterize the synthesized nanoparticles, a range of analytical tools was used. These included UV-Visible spectroscopy for optical properties, XRD for crystallinity, and SEM for surface morphology. Additional, FTIR was used to identify functional groups while PSA was used to provide insights into size distribution and monodispersity. From the result obtained, UV-Vis spectra confirmed the presence of surface plasmon resonance. Its absorption peaks ranges between 210–800 nm for CuNPs and 230–770 nm for FeNPs, respectively. XRD showed diffraction peaks confirming crystalline CuNPs, Cu_2O, FeNPs, and Fe_2O_3. The particle sizes ranges from 18.87 to 19.66 nm. SEM analysis on the other hand revealed irregularly shaped particles averaging 26.1 nm, while FTIR spectra identified functional groups such as O–H, C=O, and N–H. These functional groups confirms the involvement of polyphenols and other phytochemicals in nanoparticle synthesis. PSA results showed that 0.01 M concentrations produced well dispersed CuNPs and FeNPs with sizes of 44.61 nm and 45.89 nm, respectively. These findings confirm that *S mombin* is an effective, eco-friendly option for producing metal nanoparticles with potential uses in antimicrobial applications.

Keywords: Biosynthesis, Characterization, Copper nanoparticles, Iron nanoparticles, *Spondias mombin*

Introduction

In recent years, green approach to nanotechnology has become vital in tackling environmental, biomedical, and industrial challenges [1-2]. Conventional approaches such as chemical and physical methods for nanoparticle synthesis has caused adverse environmental impacts [3-4]. Even though this methods are effective, it often involve the uses of toxic reagents and high energy demands [4]. Consequently, due to the growing interest in environmental concern and sustainable approaches for synthesizing metallic nanoparticles (NPs) [1]. A green approach using plants part has emerge as a promising alternative [5-6].

Among the diverse biomaterials explored for green synthesis, it is obvious that *Spondias mombin*, is on the spotlight. This is because, it is a tropical plant rich in bioactive phytochemicals. Its usefulness arises due to its antioxidant, antimicrobial, and metal chelating properties [7-8]. The production of metal-based nanoparticles, such as copper (CuNPs) and iron (FeNPs), can be carried out in an ecofriendly manner [4]. This is achieved by using *S. mombin* leaf extract as a reducing and stabilizing agent [9-10].

The nanoparticles produced is widely used for water treatment, catalysis, drug delivery, and antimicrobial aided drugs [8]. This application is due to their high surface area to volume ratio, tunable physicochemical properties, and biocompatibility [2,11]. Even though literatures has addressed the effectiveness of plant mediated synthesis routes, there remains a significant knowledge gap. These gaps arise due to inadequate details in the characterization and optimization of nanoparticles derived from *S. mombin* [12-13]. Moreover, comparative evaluations of particle size and crystallinity associated with biosynthesized CuNPs and FeNPs remain underreported [14-15].

In addition to the above-mentioned evaluation, morphological features and functional groups are also lacking insight [15]. However, the purpose of this study is to synthesize and characterize copper and iron nanoparticles using *Spondias mombin* leaf extract. The study does not only provides a comprehensive physicochemical profile of the synthesized nanoparticles. Further, it explores how concentration dependent variations influence particle morphology and dispersion. By bridging these gaps, the research contributes to the growing field of plant based nanomaterials and opens new possibilities for their application in sustainable technologies [15].

Materials and Methods

Materials

All reagents used in this study were of analytical grade and employed without further purification [16]. Fresh leaves of *S. mombin* were used as the biological source for nanoparticle synthesis. Absolute ethanol (99%) served as the extraction solvent. Copper nitrate [$Cu(NO_3)_2$] and iron(II) chloride ($FeCl_2$) were used as metal precursors for the synthesis of copper and iron nanoparticles, respectively [17]. Potassium bromide (KBr) and

Nujol were utilized for sample preparation in Fourier Transform Infrared (FTIR) spectroscopy.

Distilled and tap water were used for initial washing and cleaning procedures. Syringe filters (0.22 µm and 0.45 µm) were employed to remove large aggregates during particle size analysis [18]. Instrumentation employed for characterization included a rotary evaporator for solvent removal and concentration of the plant extract. UV-visible spectral analysis was conducted using an Apel PD30000UV spectrophotometer [19].

An X-ray diffractometer (Model: XDS 200, China) running at 40 kV and 30 mA with CuKα radiation was used to evaluate the crystallographic properties [20]. A Quorum Technologies Q150R coater was used to apply the gold sputter coating, and a scanning electron microscope (SEM, Phenom ProX, PhenomWorld, Netherlands) was used to examine the morphological features [18].

FTIR spectra were acquired using a Buck 530 infrared spectrophotometer over a wavelength range of 600–4000 cm^{-1}. A Zetasizer Nano (Model: ZS-N90, Malvern Instruments, England) was used to measure the particle size distribution, polydispersity index (PDI), and Z-average diameters. It was run at 25°C with a 90° scattering angle [21]. To guarantee the accuracy and reproducibility of the findings, every measurement was carried out three times [20].

Extraction of *Spondias mombin* Leaf

Fresh *Spondias mombin* leaves were washed, dried, and ground into powder [8]. Fifty grams of the powder were extracted using cold maceration in ethanol, followed by percolation, filtration, and evaporation. The resulting extract was stored at 4°C for further use [8, 22].

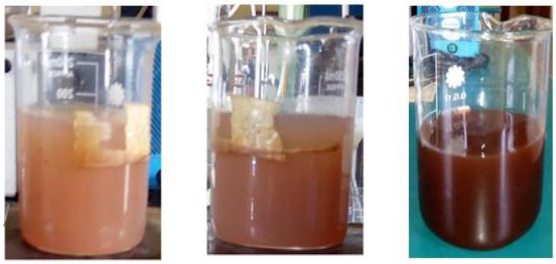

Fig 1: Colour change indicating formation of nanoparticles from light brown to dark brown

Synthesis of CuNPs and FeNPs using *Spondias mombin*

Five grams of *Spondias mombin* extract was added to 0.01 M $Cu(NO_3)_2$ and $FeCl_2$ solutions, with optimal nanoparticle formation observed at a 1:2 (v/v) ratio after heating at 90°C, indicated by color changes [23]. Reduction was confirmed via UV-Visible spectroscopy, and nanoparticles were collected by centrifugation and drying. The process was repeated for 0.02 M and 0.03 M concentrations, and the nanoparticles were later characterized [8].

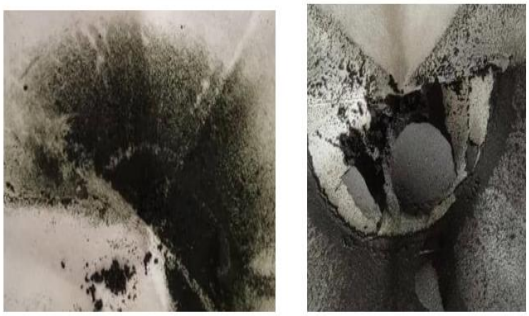

Fig 2: Synthesized *Sm*-FeNPs and *Sm*-CuNPs

Characterization of CuNPs and FeNPs using *Spondias mombin*

UV-Vis Spectroscopic Analysis

The samples were subjected to UV-visible spectrophotometric analysis using a 10-mm cell at room temperature and a UV-visible spectrophotometer (Apel PD30000uV) with a slit width of 2 nm [24]. Ten milliliters of ethanol were used to dissolve 0.1 grams of the sample. After filtering the mixture, the filtrate was used for UV-vis analysis. A UV-Spectrophotometer was used to analyze the extract under visible and UV light with wavelengths between 190 and 800 nm [25].

X-Ray Diffraction Analysis

To achieve a 10-µm particle size fraction, the sample underwent size-reduction procedures. After being ground into a powder, 0.1 g of the material was placed in a sample tray and subjected to XRD analysis (Model: XDS 200, China) [26]. A set of minerals' quantitative data is provided by the XRD analysis. The location and intensity of peaks on the 2θ scale were used to identify the minerals. An X-ray diffractometer was used to scan the prepared samples using CuKα radiation at 40 kV and 30 mA [25]. A continuous scan mode from 2 to 34° 2θ with a 0.05 step size and 2 degrees per minute was used for most of the scans [27]. Software called Jade 9+® was then used to analyze the gathered data. The process was completed by compiling the results into easily readable spreadsheets and converting each sample's XRD trace into a.jpg image radiation at 40 kV and 30 mA [27].

Scanning Electron Microscopy

PhenomWorld Einhoven, Netherlands, used the scanning electron microscope (SEM) model Phenom ProX, which was manufactured in the Netherlands, to investigate the physical structure change of samples [28]. A sample weighing 0.1 g was put on double adhesive mounted on a sample stub, which had been sputter-coated with a 5 nm layer of gold using a Quorum Technologies model Q150R. It was then brought to the SEM-EDX machine's chamber, where it was viewed using NaVCaM for focusing and minor adjustments [27]. After that, it was moved to SEM mode, where it was automatically focused and had its brightness contrast adjusted. The morphologies of various magnifications were then obtained [29].

Fourier Transform Infra-Red Analysis

To prepare the sample for the Buck 530 IR-spectrophotometer, 0.1 g of the sample was combined with 0.5 g of Kbr. Next, 1 ml of nujol, a solvent, was added to the sample using a syringe to create a paste. The sample was then placed into the instrument sample mold and allowed to scan at a wavelength of 600–4000 nm to determine its wavelength [30–31].focusing and minimal modification, it was then moved to SEM mode, where the morphologies of various magnifications were obtained after the focus and brightness contrast were automatically adjusted [29].

Particle Size Analysis

The sample was first prepared by creating a dilute suspension of the nanoparticles, with concentration

of 0.1 mg/ml levels adjusted to ensure a good signal without multiple scattering [32]. The sample was filtered through a 0.22 µm or 0.45 µm syringe filter to remove large aggregates. The appropriate dispersion medium was selected based on the solubility and stability of the nanoparticles [30].

The Zetasizer Nano (Model: ZS-N90 Malvern Instruments, England) was then calibrated using a standard sample to ensure accurate measurements [33]. Relevant parameters, such as the refractive index of the sample material and the viscosity of the dispersion medium, were input into the instrument's software [31]. The temperature was set at approximately 25°C. A clean cuvette was selected and filled with 1–1.5 ml of the prepared sample, ensuring the absence of air bubbles. The cuvette was carefully placed into the sample holder of the Zetasizer, aligned for proper measurement [29].

The measurement process involved setting the number of runs and the measurement angle, typically at 90°. The analysis was initiated, and data on the size distribution, Polydispersity Index (PDI), and Z-average diameter were recorded. The procedure was repeated in triplicate to ensure the reproducibility of the results [32].

Results and Discussion

The synthesized copper and iron nanoparticles were subjected to a comprehensive suite of analytical characterizations to evaluate their structural, morphological, and functional properties [34]. The results obtained from UV Vis spectroscopy, X-ray diffraction (XRD), scanning electron microscopy (SEM), Fourier transform infrared spectroscopy (FTIR), and particle size analysis (PSA) are presented and discussed in this section [30]. These findings provide critical insights into the impact of precursor concentration on nanoparticle formation and quality, and highlight the suitability of *Spondias mombin* as a bio-reducing and stabilizing agent in green nanotechnology [35].

The application of UV-Visible spectroscopy remains a fundamental and non-destructive technique for the preliminary characterization of metallic nanoparticles, particularly in confirming their formation and assessing their optical properties [36]. This technique is well known for detecting surface plasmon resonance (SPR) phenomena, which are caused by the collective oscillation of conduction electrons in metallic nanoparticles when they are excited by particular wavelengths of light [28].

The absorption peaks' location, form, and intensity reveal important information about the size, makeup, and aggregation behavior of the particles [30]. The optical reactions of the produced copper and iron nanoparticles at different concentrations were assessed in this work using UV-visible spectroscopy. Each metal nanoparticle system's surface plasmon behavior was then ascertained by analyzing the obtained absorption spectra [24].

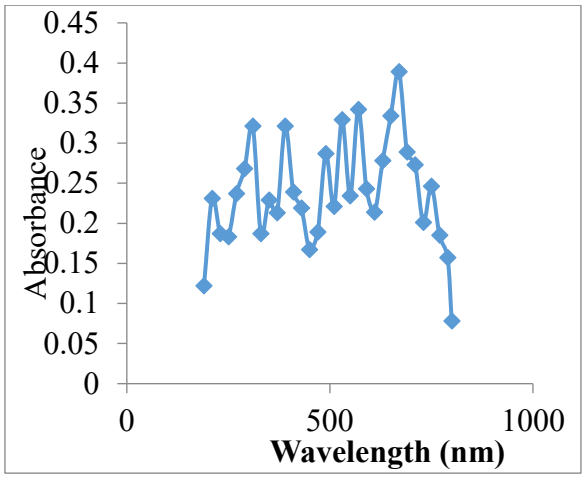

Fig 3: UV-Vis spectrum of 0.01 M *Sm*-Copper Nanoparticle

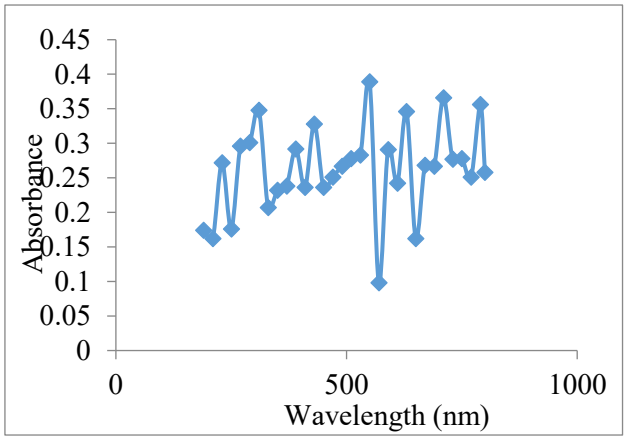

Fig 4: UV-Vis spectrum of 0.02 M *Sm*-Copper Nanoparticle

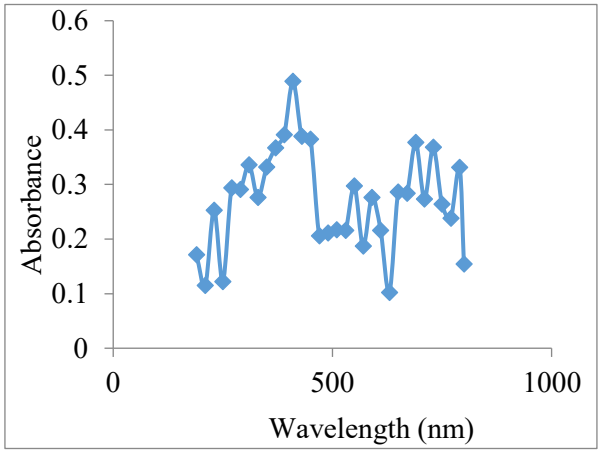

Fig 5: UV-Vis spectrum of 0.03 M *Sm*-Copper Nanoparticle

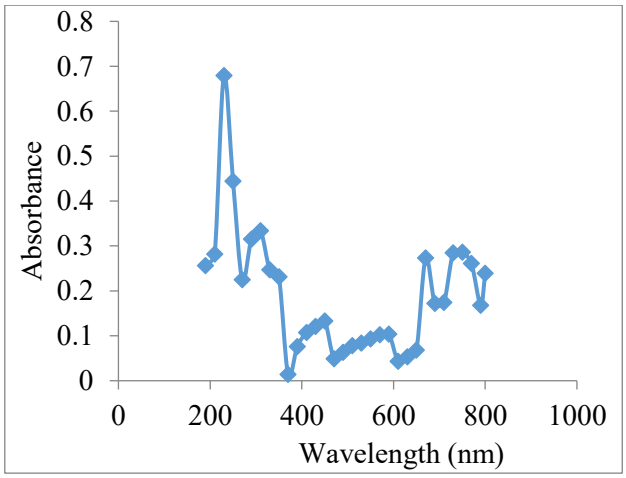

Fig 6: UV-Vis spectrum of 0.01 M *Sm*-Iron Nanoparticle

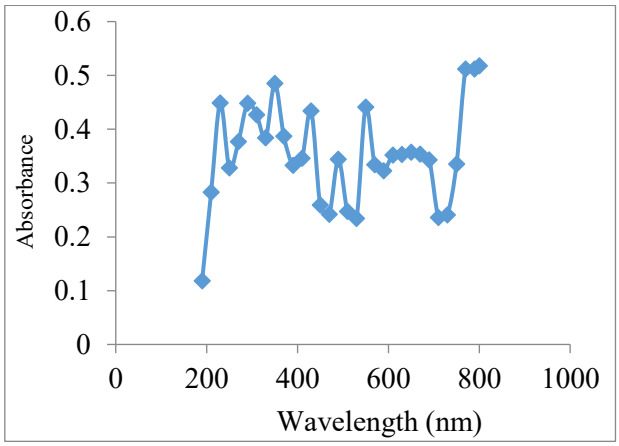

Fig 7: UV-Vis spectrum of 0.02 M *Sm*-Iron Nanoparticle

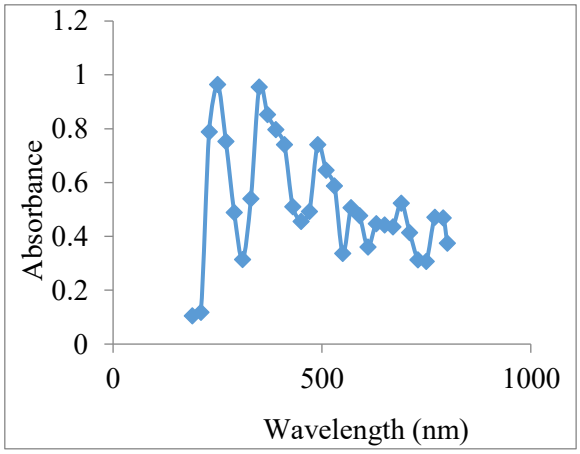

Fig 8: UV-Vis spectrum of 0.03 M *Sm*-Iron Nanoparticle

It was found that the excitation of surface plasmon vibrations in the nanoparticle solution was responsible for the absorption peaks at 210-800 nm regions for 0.01 M, 0.02 M, and 0.03 M Sm-CuNPs and 230-770 nm regions for 0.01 M, 0.02 M, and 0.03 M Sm-FeNPs in Figures 3-8. These peaks were identical to the UV-visible spectrum characteristics of CuNPs and nZVI [9,10]. According to the earlier study by [12], the visual appearance and UV-visible spectroscopy technique which is commonly used to characterize metal nanoparticles and provide a convenient identity were used to confirm the presence of copper nanoparticles. According to the findings of [37–38], inter-band transitions were seen in the CuNPs and FeNPs spectra. This demonstrated the broad range of absorption spectra of synthesized particles and the strong evidence that UV-visible spectroscopy measurements offer for detecting the presence of copper and iron nanoparticles [34].

X-ray diffraction (XRD) is a critical technique for identifying the crystalline structure, phase composition, and average crystallite size of nanomaterials [39]. It provides essential insights into the purity, structural integrity, and degree of crystallinity of synthesized nanoparticles. The analysis of diffraction patterns enables the detection of specific metal and oxide phases, as well as the estimation of particle dimensions through established models such as the Debye-Scherrer equation [40]. In this study, XRD was employed to characterize the structural properties of the biosynthesized copper and iron nanoparticles derived from *Spondias mombin* extract [8]. The diffraction peaks observed were examined to determine the presence of elemental and oxidized forms of copper and iron, assess crystallinity, and infer the potential for antimicrobial application [39].

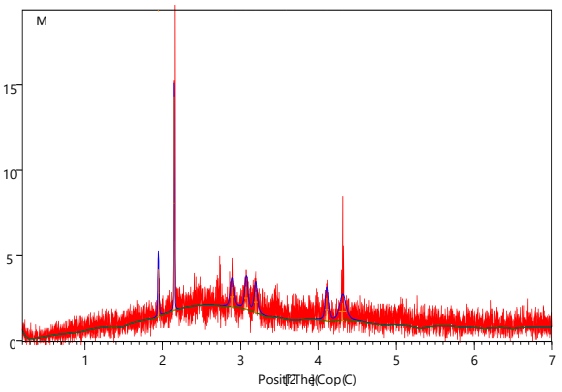

Fig 9: XRD pattern of 0.01 M *Sm*-Copper Nanoparticle

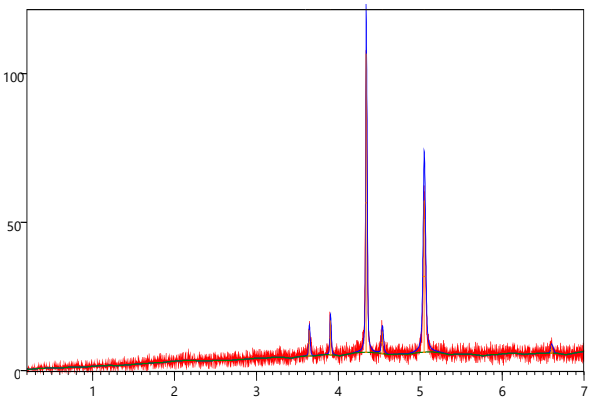

Fig 10: XRD pattern of 0.01 M *Sm*-Iron Nanoparticle

The X-ray diffractogram in Figure 9 revealed that the peak at 2Θ equals to 21.48° indicates the presence of CuNPs and 2Θ = 19.48° peak revealed the presence of CuO or Cu_2O in *Sm*-CuNPs. Similarly, the diffractogram in Figure 10 showed that nZVI is present at the peak at 2Θ equal to 43.41o. The presence of Fe2O3 or Fe3O4 was

further demonstrated by the XRD results of Sm-nZVI at the 2Θ = 39.04o peak. Other peaks, on the other hand, might represent organic matter, iron oxyhydroxides, and copper hydroxide on the surfaces of Sm-CuNPs and Sm-nZVI. The outcome was discovered to be strikingly similar to those of [3,5,6,7,9,11, 41-45]. The XRD result also revealed the presence of medium nanoparticles (10-100 nm) having crystal size, L ranging from 24-26 nm (26 nm) and particle size, D ranging from 18-19 nm (18.87 nm) for 0.01 M CuNPs and crystal size, L ranging from 25-27 nm (26.17 nm) and particle size, D ranging from 18-21 nm (19.66 nm) for 0.01 M FeNPs [2]. This has shown that *Sm*-CuNPs and *Sm*-nZVI could be promising matrix for remediation (both soil and water), adsorption, catalysis, and other applications.

Scanning Electron Microscopy (SEM) is widely utilized in nanomaterials research to visualize surface morphology, particle shape, and distribution at the nanoscale [46]. This technique provides high resolution images that enable detailed observation of nanoparticle structures, including the presence of agglomerates, surface textures, and spatial arrangements. When combined with complementary techniques such as XRD, SEM aids in confirming particle morphology and correlating it with crystallographic properties [47]. In this study, SEM analysis was employed to examine the surface architecture and size variability of the copper and iron nanoparticles synthesized using *Spondias mombin* extract [37]. The micrographs provided visual evidence of particle distribution, uniformity, and structural irregularities essential for assessing material suitability for further applications [46].

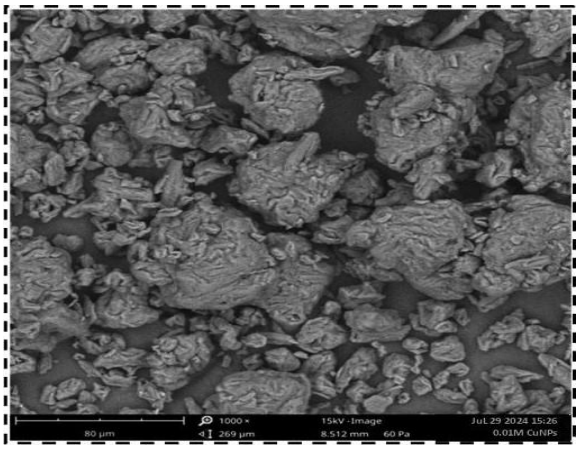

Fig 11: SEM micrograph of 0.01 M *Sm*-Copper Nanoparticle

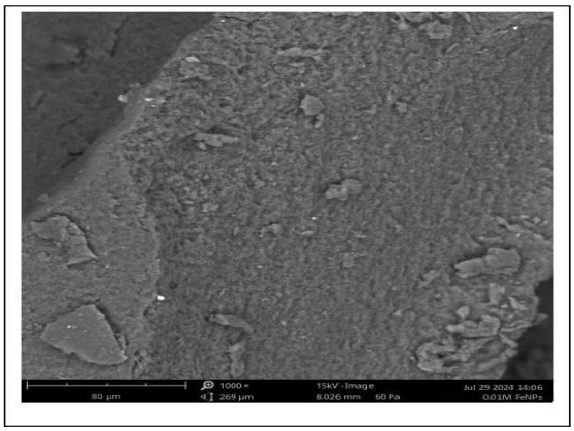

Fig 12: SEM micrograph of 0.01 M *Sm*-Iron Nanoparticle

The micrograph in Figures 11 and 12 revealed a uniform and non-uniform particle sizes and void space for both 0.01 M CuNPs and FeNPs. The particles were discovered to be irregular in form, with sizes varying from 24 to 27 nm, with an average particle size of 26.1 nm. However, XRD results revealed the crystals formed to be anisotropic [14] and lamellar or platy in shape since

the shape factor (K) was 0.7. The findings were found to be similar to those of [48-51].

Fourier Transform Infrared Spectroscopy is an essential analytical technique for elucidating the chemical composition of nanomaterials, particularly in identifying the organic functional groups involved in nanoparticle synthesis [52]. In green nanotechnology, FTIR plays a crucial role in confirming the presence of phytochemical constituents responsible for the bioreduction and stabilization of metal ions [53]. By detecting molecular vibrations associated with specific bond types, this technique enables researchers to infer the nature of interactions between plant metabolites and metal precursors. In the present study, FTIR analysis was utilized to investigate the functional groups in *Spondias mombin* extract that contribute to the formation of copper and iron nanoparticles, providing insight into the biomolecular mechanisms underlying the synthesis process [52].

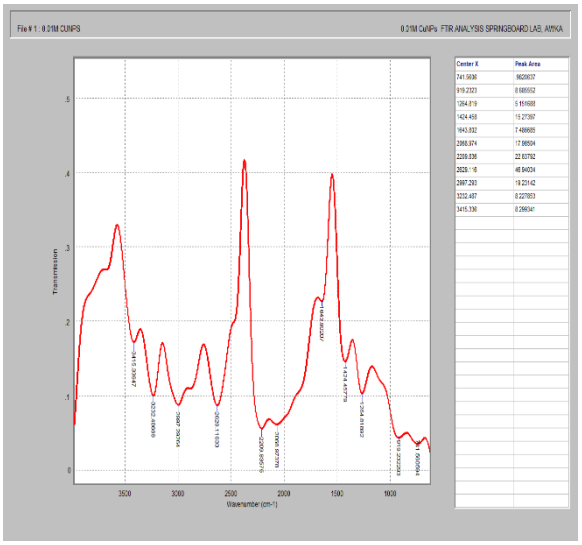

Fig 13: FT-IR vibrational bands of 0.01 M *Sm*-Copper Nanoparticle

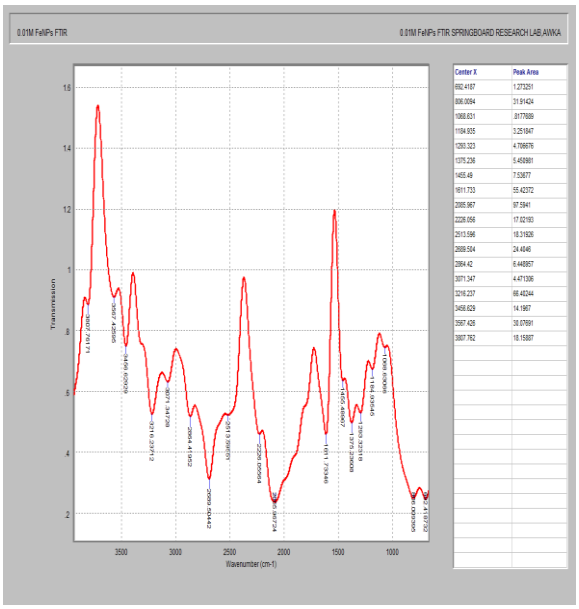

Fig 14: FT-IR vibrational bands of 0.01 M *Sm*-Iron Nanoparticle

FTIR Spectroscopy was employed to identify the presence of functional groups responsible for the synthesis of CuNPs and FeNPs from an aqueous extract of *S. mombin* leaf [40]. The vibrational bands of CuNPs and FeNPs was in the range of wave region between 600 and 4000 cm^{-1}as presented in Figures 13 and 14. The FT-IR spectra displayed three (3) distinct characteristics peaks at 1534.13, 2419.48 and 3707.67 cm^{-1} for 0.01 M *S. mombin*-CuNPs while 1533.61, 2369.83 and 3687.6 cm^{-1} for 0.01 M *S. mombin*-FeNPs. The vibrational band at 3707.67 cm^{-1} and 3687.6 cm^{-1} revealed the O-H stretching due to the presence of polyphenol or alcohol as functional group in addition to flavonoids, alkaloids, and others which may be responsible for the reduction of copper (II) ion (Cu^{2+}) to CuNPs or Cu_2O and ferrous ion (Fe^{3+}) to zero-valent iron (Fe^0). The peaks at 2419.48 and 2369.83 cm^{-1} confirmed the presence of C-H

stretching due to the alkane functional group [29]. The vibrational bands at 1534.13 and 1533.61 cm^{-1} represent bending vibration of secondary N-H, C-O stretching, C=C stretching due alkenes, and C=O stretching due carbonyl group respectively. However, the FT-IR results displayed varied vibrational bands from 694-919 cm^{-1}, 1068-1611 cm^{-1}, 2065-2997 cm^{-1} and 3071-3807 cm^{-1} representing C=C, C-O, C-N, N-H, C=O, C-H, and OH functional groups which played vital role in the synthesis of CuNPs and FeNPs. The above results were very close to the work of [15]. Moreover, similar FT-IR patterns were found in the following studies: biologically synthesized iron nanoparticles (FeNPs) from Phoenix dactylifera; green synthesis of iron nanoparticles and their environmental applications and implications; green synthesis of copper nanoparticles using leaf extract from Ocimum sanctum; green synthesis of iron nanoparticles using aqueous extract of Musa ornata flower sheath against pathogenic bacteria; antifungal activity of biosynthesized copper nanoparticles evaluated against red root-rot disease in tea plants; etc revealed similar FT-IR pattern [3,5,6,9,10,13,54].

Understanding the particle size distribution of nanoparticles is essential for evaluating their physicochemical behaviour and functional suitability in various applications [55]. Particle size influences not only the surface reactivity and stability of nanoparticles but also their dispersion, aggregation tendency, and interaction with biological and environmental systems. In nanoparticle synthesis, precise measurement of particle dimensions and distribution patterns provides key indicators of synthesis efficiency and reproducibility. In this study, particle size analysis was conducted to assess the consistency and uniformity of the copper and iron nanoparticles synthesized using *Spondias mombin* extract, with particular attention to how concentration affects size distribution and polydispersity [56].

Table 1: Particle Size Areas of *Sm*-Copper and Iron Nanoparticles

S/N	***Sm*-Nanoparticles**	**PSA (nm)**	**Polydispersity Index**	**Length unit**
1	0.01M CuNPs	44.61	0.268	DV (10)
2	0.02M CuNPs	19.05	0.300	DV (10)
3	0.03M CuNPs	14.40	0.461	DV (10)
4	0.01M FeNPs	45.89	0.199	DV (10)
5	0.02M FeNPs	28.86	0.214	DV (10)
6	0.03M FeNPs	24.17	0.478	DV (10)

*DV (10) represents that 10% of particles in the powders are smaller than this size

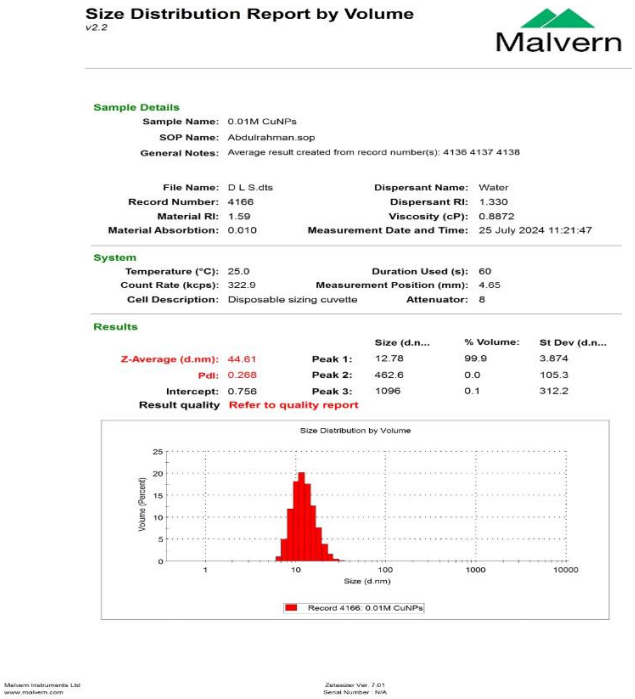

Fig 15: Particle size distribution of 0.001 M CuNPs

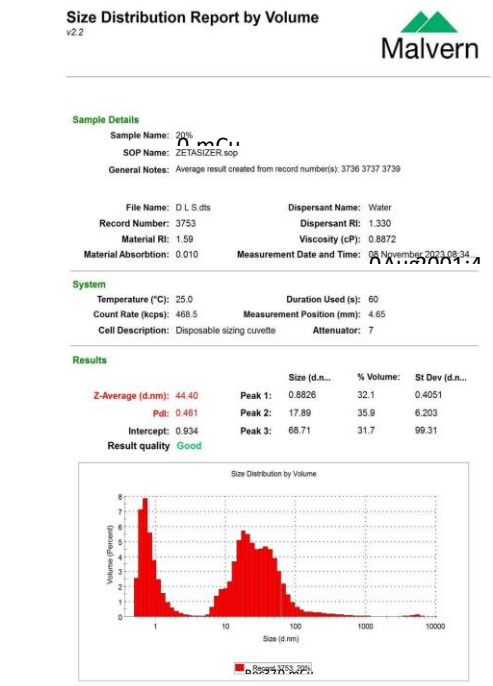

Fig 17: Particle size distribution of 0.003 M CuNPs

Fig 16: Particle size distribution of 0.002 M CuNPs

Fig 18: Particle size distribution of 0.001 M FeNPs

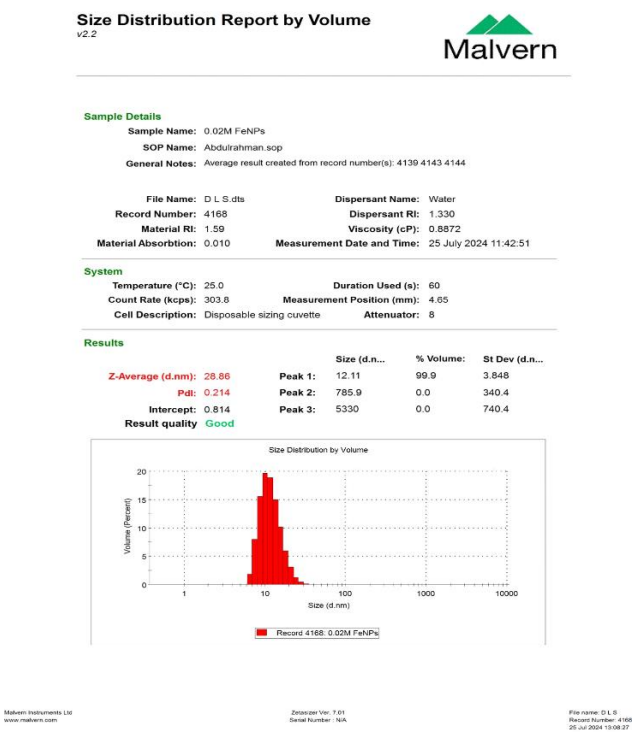

Fig 19: Particle size distribution of 0.002 M FeNPs

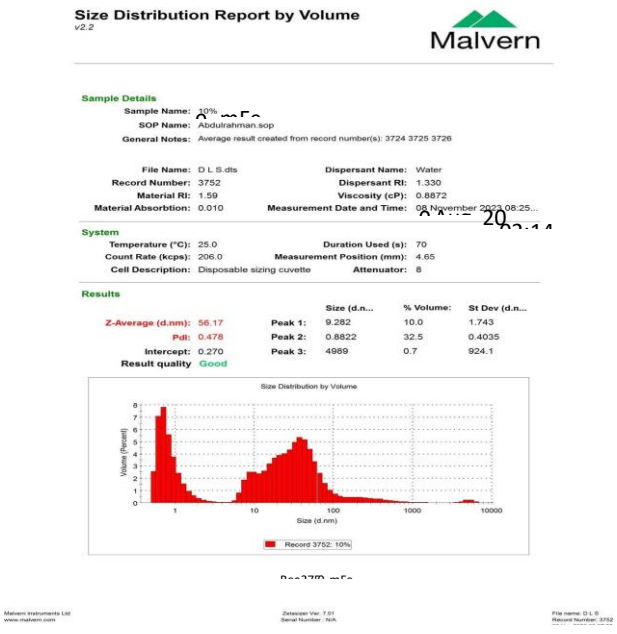

Fig 20: Particle size distribution of 0.003 M FeNPs

Particle size is a veritable parameter in material composition, identity, quality, and performance. The size of the particle's controls flows and compaction properties [34]. The particle size area as a function of the total surface area and polydispersity Index (PdI) in Table 1 revealed that 0.001 M of both CuNPs and FeNPs gave the highest PSA of 44.61 nm and 45.89 nm demonstrating the use of 0.01 M CuNPs and FeNPs in subsequent analyses. The PSD results for CuNPs and FeNPs revealed that the particles were found to be in the nano scale and highly monodispersed [1]. The Distribution particle size by volume revealed that all the concentrations of both CuNPs and FeNPs particles in the powders were 10% smaller than this size as shown in Figures 15-20.

Conclusion

This work used leaf extract from *Spondias mombin* to demonstrate the environmentally friendly synthesis of copper and iron nanoparticles (CuNPs and FeNPs). The plant extract acted as a stabilizing and reducing agent that was sustainable [57]. XRD, SEM, FTIR, UV-Vis spectroscopy, and particle size analysis were used to confirm the presence of nanoparticles. Surface plasmon resonance bands were visible in UV-Vis spectra. Crystalline structures containing peaks for elemental and oxidized copper and iron were found using XRD [58]. Heterogeneous shapes with sizes ranging from 18 to 27 nm were revealed by SEM. Functional groups (O-H, C-H, N-H, and C=O) were detected by FTIR, indicating phytochemical involvement. At

lower precursor concentrations, particle size analysis revealed monodispersity and low polydispersity. The process is economical, environmentally benign, and appropriate for environmental remediation, catalysis, and antimicrobial activity [59]. Overall, this study provides a scientific basis for the detailed physicochemical characterization of *Spondias mombin*-mediated nanoparticles and supports its potential use in sustainable nanomaterial synthesis.

Acknowledgement

The authors thank the Springboard Research Laboratory, Awka Anambra State, for the characterization facilities.

Conflict of Interest Statement

The authors declare that there is no competing interest related to this work.

Data Availability Statement

All relevant data supporting the findings of this study are available from the first or corresponding author upon reasonable request.

References

[1] Khan, I., Saeed, K., & Khan, I. (2019). Nanoparticles: Properties, Applications and Toxicities. *Arabian Journal of Chemistry,* 12(2), pp. 908–931.

[2] Ayomide, B. O., Obi, C., & Obuzor, G. U. (2023). Follow-Up Application of *Spondias Mombin* Modified Nano-Sorbent for Trace Metals Remediation. *American Journal of Physical Chemistry,* 12(1), pp. 1-6.

[3] Saif, S., Tahir, A., & Chen, Y. (2016). Green Synthesis of Iron Nanoparticles and their Environmental Applications and Implications. *Nanomaterials, 6*(2), pp. 209-220.

[4] Mondal, P., Anweshan, A., & Purkait, M. K. (2020). Green Synthesis and Environmental Application of Iron-based Nanomaterials and Nanocomposite: A Review. *Chemosphere,* 259(5), pp. 127-140.

[5] Saranya, S., Vijayarani, K., & Pavithra, S. (2017). Green Synthesis of Iron Nanoparticles using Aqueous Extract of *Musa Ornate* Flower Sheath against Pathogenic Bacteria. *Indian Journal of Pharmaceutical Science,* 79(5), pp. 688-694.

[6] Eldeeb, B. A., El-Raheem, W. A., & Elbeltagi, S. (2023). Green Synthesis of Biocompatible Fe_3O_4 Magnetic Nanoparticles using *Citrus Sinensis* Peels Extract for their Biological Activities and Magnetic-hyperthermia Applications. *Scientific Reports,* 13(2), pp. 190.

[7] Ilangovan, R., Subha, V., Earnest, R.S., Kirubanandan, S., Renganathan, S. (2021). Nanomaterials: Synthesis, Physicochemical Characterization, and Biopharmaceutical Applications. *Elsevier,* 13(2), pp. 33-70.

[8] Eze, U. S, Obi, C, & James, A. O. (2024). Quantification of Phytochemical Constituents of Ethanol Yellow Spondias mombin Leaf Extract in Ogba/Ebgema/Ndoni Local Ethanol Yellow Spondias mombin Leaf Extract in Ogba/Ebgema/Ndoni Local Government Area of Rivers State, Nigeria. *Journal Applied Sciencec and Environmental Management*, 28 (8), pp. 2557-2574.

[9] Ponnusamy, P., Kolandasamy, M., Viswanathan, E., & Balasubramanian, M. G. (2016). Antifungal Activity of Biosynthesized Copper Nanoparticles Evaluated against Red Root-rot Disease in Tea Plants. *Journal of Experimental Nanoscience,* 13(5), pp. 32-45.

[10] Batool, F., Iqbal, M. S., Khan, S. D., Khan, J., Ahmed, B., & Qadir, M. I. (2021). Biologically Synthesized Iron Nanoparticles (FeNPs) from Phoenix Dactylifera have

Anti-bacterial Activities. *Scientific Reports,* 11(1), pp. 22132.

[11] Mohamed, A., Atta, R. R., & Kotp, A. A. (2023). Green Synthesis and Characterization of Iron Oxide Nanoparticles for the Removal of Heavy Metals (Cd^{2+} and Ni^{2+}) from Aqueous Solutions with Antimicrobial Investigation. *Scientific Reports*, 13(7), pp. 7227.

[12] Krithiga, N., Jayachitra, A., & Rajalakshmi, A. (2013). Synthesis, Characterization and Analysis of the Effect of Copper Oxide Nanoparticles in Biological Systems. *Industrial Journal of Nanoscience*, 1(3), pp. 6-15.

[13] Vasudev, D.K., & Pramod, S.K. (2013). Green Synthesis of Copper Nanoparticles using *Ocimum Sanctum* leaf extract. *International Journal of Chemical Studies*, 1(3), pp. 1-4.

[14] Pearce, A.K., Wilks, T.R., & Arno, M.C. (2021). Synthesis and Applications of Anisotropic Nanoparticles with Precisely Defined Dimensions. *Nature Reviews Chemistry,* 5(1), pp. 21-45.

[15] Monalisa, P., Sudipta, S., & Tapas, K. B. (2013). Plant Extract Mediated Green Synthesis of Silver Nanoparticles using *Allium Cepa* Extract and its Antimicrobial Activity. *Applied Nanoscience*, 3(5), pp. 303–308.

[16] Ali, M., Ahmed, S., & Khan, T. (2020). Green Synthesis of Metallic Nanoparticles using Plant Pxtracts: A Review on Current Trends and Future Perspectives. *Journal of Advanced Research in Nanoscience and Nanotechnology*, 6(2), pp. 15–22.

[17] Zhao, Y., Liu, X., & Wang, Y. (2021). Synthesis and Applications of Metal Nanoparticles using Inorganic Precursors: A Systematic Overview. *Materials Chemistry and Physics*, 270 (5), pp. 124-138.

[18] Mehta, M., Kulkarni, A., & Yadav, P. (2022). Size Characterization of Nanoparticles using Dynamic Light Scattering and Nanoparticle Tracking Analysis. *Materials Today: Proceedings*, 56(3), pp. 1345–1350.

[19] Chen, H., Zhang, M., & Zhao, Y. (2020). Application of UV-Vis Spectroscopy in the Characterization of Green Synthesized Metal Nanoparticles. *Journal of Analytical Science and Technology*, 11(1), pp. 45–53.

[20] Wang, J., & Lee, C. Y. (2021). Crystallographic Studies of Metal Nanoparticles using X-ray Diffraction: Principles and Recent Advances. *Crystallography Reviews*, 27(1), pp. 1–14. [21] Nguyen, T. T., Vo, T. T., & Le, H. T. (2019). Characterization Techniques for Nanoparticles: Comparison and Evaluation. *Journal of Nanomaterials and Molecular Nanotechnology*, 8(3), pp. 1–6.

[22] Sofowora, A. (1993). Phytochemical Screening of Medicinal Plants and Traditional Medicine in Africa Edition. *Spectrum Books Ltd*., Nigeria, pp. 150-156.

[23] Khan, I., Saeed, K., & Khan, I. (2018). 'Nanoparticles: Properties, Applications, and Toxicities'. *Arabian Journal of Chemistry*, 12(7): 908-931.

[24] Singh, A., & Patel, R. K. (2020). Optical Analysis of Metal Nanoparticles using UV-Vis Spectroscopy. *Materials Today: Proceedings*, 28(4), pp. 1235–1240.

[25] Rahman, M. M., Hossain, M. S., & Ahmed, T. (2021). UV-Vis Spectroscopy: A Reliable Technique for Nanoparticle Characterization. *Asian Journal of Nanoscience and Materials*, 4(1), pp. 35–42. [26] Zhang, Y., Li, H., & Chen, Q. (2021). Recent Advances in the XRD Analysis of Nanopowders and Crystalline Materials. Journal for *Crystals Chemistry*, 11(2), pp. 137-150.

[27] Kumar, R., & Bera, A. (2020). X-ray Diffraction Techniques for Characterization of Nanomaterials: A comprehensive Review. *Journal of Materials Research and Technology*, 9(6), pp. 14700–14715.

[28] Brown, A. L., Rodriguez, M., & Okafor, U. (2021). Scanning Electron Microscopy for Nanomaterials: Techniques and Considerations. *Microscopy and Microanalysis Research*, 27(4), pp. 312–318. [29] Lee, S. H., & Chen, Y. M. (2020). Advances in Sputter Coating for High-Resolution SEM Imaging of Nanoparticle Surfaces. *Journal of Surface Science and Technology*, 36(1), pp. 29–36.

[30] Adeyemi, T. M., & Zhang, Y. (2021). Application of FTIR in the Structural Elucidation of Biomolecule–nanoparticle Interactions. *Spectroscopy Letters*, 54(2), pp. 147–156.

[31] Martins, J. T., Cerqueira, M. A., & Vicente, A. A. (2020). Fourier Transform Infrared Spectroscopy for the Analysis of Polysaccharide Nanocomposites: Sample Preparation and Measurement Protocols. *Carbohydrate Polymers*, 228(4), pp. 115-139.

[32] Garcia, C. P., Almeida, M. F., & Silva, J. R. (2021). Preparation and Analysis of Nanoparticle Suspensions for Dynamic Light Scattering Measurements. *Nanotechnology Reviews*, 10(1), pp. 241–251.

[33] Nguyen, L. H., & Vo, D. D. (2020). Principles and Practices of Nanoparticle Size Characterization using DLS and Zeta Potential Techniques. *Journal of Applied Nanoscience and Technology*, 8(3), pp. 101–109.

[34] Patel, H. R., Desai, M. A., & Trivedi, R. (2021). Multi-technique Characterization of Phytomediated Metallic Nanoparticles and their Relevance to Green Chemistry. *Applied Nanoscience*, 11(4), pp. 1345–1357.

[35] Lopez, M. A., & Sharma, R. (2020). Green Synthesis and Characterization of Metal Nanoparticles using Plant Extracts: A Review of Current Trends. *Materials Today: Proceedings*, 33(3), pp. 4567–4572.

[36] Chandra, S., Singh, S., & Jain, D. (2022). Optical Properties of Biosynthesized Metallic Nanoparticles using UV-Vis Spectroscopy. *Journal of Materials and Environmental Science*, 13(2), pp. 145–152.

[37] Varshney, R., Bhadauria, S., & Gaur, M.S. (2010). Characterization of Copper Nanoparticles Synthesized by a Novel Microbiological Method. *Journal of Mineral Materials Society*, 62(12), pp. 102-104.

[38] Varshney, R., Bhadauria, S., & Gaur, M.S. (2011) Copper Nanoparticles Synthesis from Electroplating Industry Effluent. *Nano Biomedical Engineering*, 3(2), pp. 115-119.

[39] Thomas, S., Joy, P. A., & George, S. C. (2021). Structural Analysis of Nanomaterials using X-ray Diffraction. *Materials Science Advances*, 6(1), pp. 33–41.

[40] Iqbal, J., & Khan, M. (2020). Crystallographic and Phase Analysis of Metal Nanoparticles using XRD Techniques. *Journal of Nanoscience and Nanotechnology Applications*, 4(2), pp. 22–28.

[41] Sun, Y.P., Li, X.Q., Cao, J., Zhang, W.X., & Wang, H.P. (2006) Characterization of Zero-valent Iron Nanoparticles. *Advance Colloid and Interface Science,* 120(1-3), pp. 47-56.

[42] Singh, K. P., Singh, A. K., Gupta, S., & Sinha, S. (2011) Optimization of Cr (VI) Reduction by Zero-valent Bimetallic Nano-Particles using the Response Surface Modeling Approach. *Desalination,* 270(1-3), pp. 275-284.

[43] Khasim, S., Raghavedra, S., Revanasiddappa, M., Sajjan, K., Sajjan, K., Mohana, L., & Faisal, M. (2011). Characterization and Magnetic Properties of Polyaniline. *Bulletin of Material Science,* 34(7), pp. 1557-1561.

[44] Mogilevsky, G., Hartman, O., Emmons, E.D., Balboa, A., DeCoste, J.B., Schindler, B.J., Iordanov, I., & Karwacki, C.J. (2014). Bottom-up Synthesis of Anatase Nanoparticles with Graphene Domains. *ACS Applied Materials & Interfaces*, 6(2), pp. 10638-10648.

[45] Qayoom, M., Shah, K.A., & Pandit, A.H. (2020). Dielectric and Electrical

Studies on Iron Oxide (α-Fe_2O_3) Nanoparticles Synthesized by Modified Solution Combustion Reaction for Microwave Applications. *Journal of Electroceramics,* 45(3), pp. 7-14.

[46] Fernandez, M. P., Oliveira, T. L., & Souza, R. F. (2021). Advances in SEM Techniques for Characterizing Biogenic and Engineered Nanoparticles. *NanoCharacterization Journal*, 9(1), pp. 55–63.

[47] Adebayo, A. R., & Lin, Y. C. (2020). High-resolution Imaging and Particle Morphology Analysis using Scanning Electron Microscopy in Nanotechnology Research. *Journal of Microscopy and Imaging Science*, 12(3), pp. 101–108.

[48] Kowshik, M., Ashtaputre, S., Sharmin, K., Vogel, W., & Urban, J. (2002). Extracellular Synthesis of Silver Nanoparticles by a Silver-tolerant Yeast Strain MKY3. *Nanotechnology,* 14(1), pp. 95.

[49] Sondia, I., & Sondi, B.S. (2004). Silver Nanoparticles as Antimicrobial Agent: A Case Study on *E. coli* as a Model for Gram-negative Bacteria. *Journal of Colloid and Interface Science,* 275(1), pp. 177-182.

[50] Kumar, R., Singh, S., & Pandey, N. (2015). Potential of Green Synthesized Zero-valent Iron Nano-particles for the Remediation of Lead-contaminated Water. *International Journal of Environmental Science and Technology,* 12(12), pp. 3943-3950.

[51] Sravanthi, K., Ayodhya, D., & Yardgiri, P. (2018). Green Synthesis, Characterization of Biomaterial Supported Zero-valent Iron Nano-particles for Contaminated Water Treatment. *Journal of Analytical Science and Technology,* 9(3), pp. 11-18.

[52] Miller, D. A., & Rahman, M. A. (2021). FTIR Spectroscopy in Nanomaterials Research: Principles and Recent Advances. *Analytical Techniques in Chemistry*, 13(2), pp. 77–84.

[53] Okeke, C. P., Ezeonu, F. C., & Ogbodo, E. N. (2020). Role of FTIR in Identifying Phytochemicals Involved in the Biosynthesis of Metallic Nanoparticles. *International Journal of Green Nanotechnology*, 8(1), pp. 22–29.

[54] Reichenbächer, M. & Popp, J. (2012). Vibrational Spectroscopy. In: Challenges in Molecular Structure Determination. *Springer, Berlin, Heidelberg*, 17(7), pp. 67-80.

[55] Torres, V. M., Delgado, A.C., & Singh, K. (2021). Advances in Nanoparticle Size Characterization: Implications for Reproducibility and Application. *Materials Characterization Journal*, 167(5), pp. 110-122.

[56] Mensah, R. A., & Zhou, L. (2020). Importance of Particle Size Analysis in Nanomaterials Design and Application. *Journal of Nanoscience Research*, 5(2), pp. 98–105.

[57] Gonzalez, L. A., Silva, F. P., & Mendez, R. A. (2022). Bio-inspired Synthesis of Metallic Nanoparticles using Tropical Plant Extracts: Recent Trends and Applications. *Environmental Nanotechnology, Monitoring & Management*, 18(7), pp. 100-117.

[58] Singh, P., & Meena, R. (2021). Structural and Functional Analysis of Plant-mediated Nanoparticles using XRD, SEM, and FTIR techniques. *Nanoscience Advances*, 3(2), pp. 102–111.

[59] Ahmed, M. Y., Li, C., & Okoro, H. (2023). Green Nanotechnology: Advances in Plant-based Synthesis and Multifunctional Applications of Metal Nanoparticles. *Sustainable Materials and Technologies*, 36(5), pp. 23-50.